RSC Advances




ROYAL SOCIETY OF CHEMISTRY

www.rsc.org/advances

Journal Name

RSCPublishing

ARTICLE

# Mesoporous $Ce_xCo_{1-x}Cr_2O_4$ spinels: Synthesis, characterization and catalytic application in simultaneous removal of soot particulate and NO

Cite this: DOI: 10.1039/x0xx00000x

Received 00th January 2012,
Accepted 00th January 2012

DOI: 10.1039/x0xx00000x

www.rsc.org/

Xiaowei Niu [a], Liang Zhou[b], Xiaojun Hu*[a] and Wei Han*[b]

Cerium-doped mesoporous spinel-type catalysts were prepared via a solution combustion synthesis method and were investigated for the catalytic combustion of soot and NO. Characterization studies using BET, XRD, SEM, TEM and catalytic activity tests confirmed that these catalysts effectively and simultaneously removed soot and NO, which are the two prevalent pollutants in diesel exhaust in the temperature range of 200-600℃. The results from the characterization indicated that the deformation of a spinel structure might occur in the process of cerium substitution. This deformation would increase the oxygen mobility and affect the catalytic performance of cerium modified spinel-type catalysts.

## 1. Introduction

In recent years, diesel engines have been widely used in many types of vehicles, such as commercial vehicles, as well as light and heavy-duty trucks, due to their high fuel efficiency, durability and reliability[1]. However, particulate matter (PM) and gas NOx are the main pollutants in the diesel exhaust [2], has drawn more attention due to effects of air quality and human health. Among these, nitrogen oxides, which contributes to urban smog and acid rain[3,4], and different soot particle sizes, especially ultrafine particles that can produce effects on different regions of the respiratory tract and cross cell membranes, enter the blood circulation and may even enter the brain[5]. Recent epidemiologic research indicates that cardiovascular and respiratory diseases are closely associated with ultrafine particles (diameter<100 nm)[6].

The automotive industry is currently facing serious challenges to reduce the environmental impact from vehicles due to the EU VI legislation

[a]*Key Lab of Regional Environment and Eco-Remediation, Ministry of Education China, Dadong District, Shenyang, 110044, China . E-mail: hu-xj@mail.tsinghua.edu.cn ; Fax: +86-24-62268101; Tel: +86-24-62268101*

[b]*College of Physics, Jilin University,Chaoyang District, Changchun, 130021, China. E-mail:whan@jlu.edu.cn; Fax: +86-431-85167869; Tel: +86-431-85167869*

for diesel cars that takes effect September 2014[7] (i.e., commercial vehicle and heavy-duty truck emissions contain less than 4.5 mg $km^{-1}$ of PM and 0.08 g $km^{-1}$ of NOx and less than 0.01 g /kWh of PM and 0.4 g /kWh of NOx, respectively.)

To solve this problem, many types of approaches for the control of NOx and PM emissions are being investigated (e.g., 8, 9). The simultaneously removal of PM and NOx in a single suitably catalyzed trap is clearly more ambitious and has been recently explored due to the considerable advantages it might provide in terms of both the investment cost and pressure drop reduction compared to that in the two stage catalyzed trap. Catalysis can play an important role and provide results similar to those obtained with a catalyzed trap in diesel engines. Therefore, the development of an appropriate catalyst is required.

Similar to other studies focused on catalysts for the combined abatement of $NO_x$ and diesel soot particulates, the activity of catalysts based on transition metal oxides, such as Cu, Mn, Fe, Co, and Cr oxides, can exhibit outstanding catalytic behavior at low temperatures, and these transition metal oxides could be substitute for precious metals[10]. $NO_x$ acts as an oxidizing agent for soot combustion[11,12]. Therefore, some cobalt-containing spinel-type catalysts have been studied as potential candidates for the simultaneous removal of two prevalent pollutants (i.e., PM and $NO_x$) in diesel exhausts[13,14]. Cobalt-containing spinel-type catalysts have attracted much attention for many years due to the relatively abundant resources and lower cost[15,16]. In addition these catalysts are very active for catalytic removal of $NO_x$ and PM[17]. It is well known that doping of a metal oxide results in a doped material that has significantly different properties than the undoped material[18,19,20]. Cerium is a well-known additive in exhaust catalysts due to its oxygen storage capacity, which can enhance the activity[21,22]. Therefore, cerium was chosen as the dopant for $CoCr_2O_4$ in the current investigation. Although, both cobalt and Cerium are widely applied to important oxidation processes, mesoporous materials of their complex oxides applications to the oxidation of diesel soot particulates are very limited.

In this study, the catalytic activity of mesoporous $Ce_xCo_{1-x}Cr_2O_4$ spinels catalysts ($CoCr_2O_4$) for the simultaneous removal of PM and NO in the presence of oxygen has been investigated. To study the catalytic activity, simulated diesel exhaust conditions are employed as the test conditions. The results from these studies suggest that cerium-doped catalysts exhibited excellent catalytic activity at a low temperature and are more suitable for the simultaneous removal of PM and NO in diesel exhausts.

## 2. Experimental

### 2.1. Catalyst preparation

A series of $Ce_xCo_{1-x}Cr_2O_4$ (x=0, 0.05, 0.1, 0.15) spinel-type samples prepared via a solution combustion synthesis from metal nitrates ($Co(NO_3)_2 \cdot 6H_2O$, $Ce(NO_3)_3 \cdot 6H_2O$, $Cr(NO_3)_3 \cdot 9H_2O$, and urea[17]. The reagents used in the experiment are all analytically pure and were purchased from Sinopharm Chemical Reagent Co.,Ltd China. Solution combustion synthesis takes advantage of the highly exothermic and self-sustaining reaction between metal nitrates and urea and has been applied to the production of nano-sized catalyst particles. The combustion synthesis process can be formally split into the following two steps:

$$xCe(NO_3)_3 + 1\text{-}xCo(NO_3)_2 + 2Cr(NO_3)_3 \rightarrow Ce_xCo_{1-x}Cr_2O_4 + \frac{8+x}{2}N_2 + \frac{20+3x}{2}O_2 \quad (1)$$

and

$$20CO(NH_2)_2 + 30O_2 \rightarrow 20CO_2 + 40H_2O + 20N_2. \quad (2)$$

To ensure proper homogeneity, the aqueous mixtures (metalprecursors and urea dosed in stoichiometric ratio) were heated and stirred for several minutes. Then, the as-prepared solution was stirring in air maintained at 80℃ for 4 h and calcined in air in an electric oven maintained at 600℃ for 4 h. The whole process of markedly exothermic was over after 5~6 min, but the time of the reacting solid mixture greatly exceeding 1000 ℃ was few seconds. Next, all of the prepared samples were ground with a mortar and pestle at room temperature. Finally, all of the prepared samples were immersed in the absolute ethanol for 30 min to enhance the dispersion of the samples, and then physical characterization and chemical activity measurement were performed.

### 2.2. Catalyst characterization

X-ray diffraction (XRD) was performed with a Japan D/max-RA diffractometer with Cu Kα radiation (I = 1.5418 Å; tube voltage, 50 kV; tube current, 150 mA). The diffraction patterns were obtained in a 2θ range of 15° to 80° at a scan step size of 0.02°. The resulting XRD profiles were analyzed to confirm the crystal phase of the prepared samples using reference standards.

Scanning electron microscopy (SEM; JEOL, JSM-5600, Japan) and transmission electron microscopy (TEM; H8160, Japan) were performed to analyze the microstructure of the crystal agglomerates and the crystals of the prepared samples.

Nitrogen adsorption was used to measure the BET surface area (ASAP 2010 apparatus).

### 2.3. Chemical activity measurement

The evaluation of catalytic activities for the simultaneous removal of PM and NOx were performed in a quartz tubular fixed-bed continuous-flow reactor (Φ=8 mm, i.d.) and evaluated using a temperature-programmed reaction. The reaction temperature was varied during each temperature-programmed reaction run from 200℃ to 600℃ at a rate of 5℃·min$^{-1}$. Printex-U from DEGUSSA Inc. was used as model soot from diesel engine exhaust.

The weight ratio of the soot particles to the catalyst was 9:1, and 100 mg of the mixture was obtained with a spatula in the loose-contact contact mode, which is somewhat consistent with the actual circumstances. Blank experiments were performed under identical conditions but without the catalysts (i.e., only in the presence of the PM).

The composition of the feed gas mixture was 1000 ppm of NO and 10 vol% of $O_2$ with $N_2$. In the activity test, the gas total flow rate was 50 ml/min. The flow was accurately measured and controlled using mass flow meters by Beijing Sevenstar Electronics Co., Ltd., China. After the reaction, the composition $O_2$, CO, $CO_2$, and NO in the gas was measured online and analyzed using a flue gas analyzer (KM9106) and a gas chromatograph (SP-3420). The NO conversion is defined by equation [23] (2.1):

$$X_{(NO)} = \frac{[NO]_{in} - [NOx]_{out}}{[NO]_{in}} \times 100\% \quad (2.1)$$

In this work, the temperature at $T_{10}$, $T_{50}$, and $T_{90}$, which are defined as the temperatures at which 10, 50, and 90% of the soot particulates were oxidized, respectively, were used to evaluate the catalytic activity.

## 3. Results and discussion

### 3.1. Characterization results

The XRD patterns of the $Ce_xCo_{1-x}Cr_2O_4$ (x=0, 0.05, 0.1, 0.15) powders of spinel catalysts are shown in Fig. 1. All the diffraction peaks of the spinel catalysts can be indexed to the (220), (311), (222), (400), (422), (511)and (440) crystal faces, which correspond to a face centered cubic (FCC) of $CoCr_2O_4$ (JPCDS 22-1084). It is important to note that the diffraction peaks of 2θ show a slight upshift from 35.8° to 36.8° with the increasing of x in $Ce_xCo_{1-x}Cr_2O_4$. This change could be primarily ascribed to the size difference between $Ce^{4+}$(0.087) and $Co^{2+}$(0.065), $Ce^{4+}$ ions enter into the spinel-type lattice of $CoCr_2O_4$, leading to the shrinkage of the lattice[24,25]. Therefore, a portion of $Co^{2+}$ in $Ce_xCo_{1-x}Cr_2O_4$ was substituted by $Ce^{4+}$, the deformation of the spinel structure might occur in the process of cerium substitution. Bueno-López et al[26] also reported that this deformation favors oxygen mobility and affects the redox behavior of the material. When the molar ratio of cerium-doped in $CoCr_2O_4$ is greater than 0.2 (or 20%) does the characteristic band of $CeO_2$ appear in the Raman spectra[27]. For higher degree of cerium substitution (x=0.15), the size of the $Ce_{0.15}Co_{0.85}Cr_2O_4$ increased. This may be attributed to the crystalline $CeO_2$ formation. In addition, the average crystallite sizes (D) of $Ce_xCo_{1-x}Cr_2O_4$(x=0, 0.05, 0.1, 0.15) catalysts were determined with the Scherrer equation,

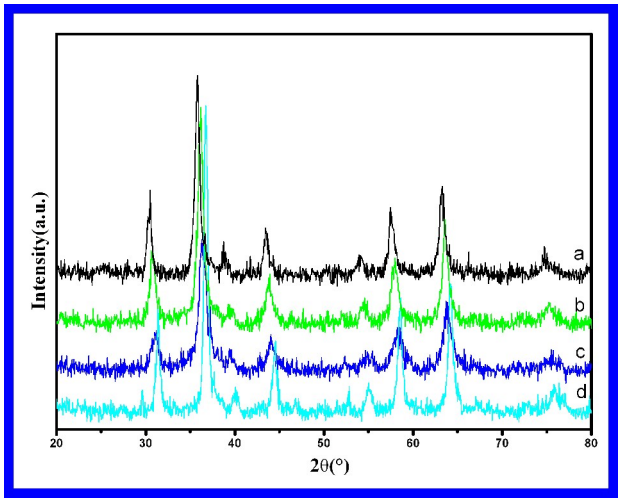


**Fig. 1.** XRD spectra of the $Ce_xCo_{1-x}Cr_2O_4$ catalysts: (a)x=0, (b)x=0.05, (c)x=0.1, (d)x=0.15.

$$D = \frac{\kappa \cdot \lambda}{\beta \cdot \cos\theta}$$

**Table 1.** Summary of $N_2$-sorption isotherm results and catalytic performance of the $Ce_xCo_{1-x}Cr_2O_4$(x=0, 0.05, 0.1, 0.15) catalysts for the simultaneous removal of soot and NO.

| Sample | $S_{BET}$ ($m^2/g$) | Total pore Volume $V_{tot}$ ($cm^3/g$) | Pore size diameter $d_{BJH}$ (nm) | crystalline size (nm) | (℃) | | | (%) |
|---|---|---|---|---|---|---|---|---|
| | | | | | $T_{10}$ | $T_{50}$ | $T_{90}$ | Xmax |
| Printex-U soot | | | | | 525 | 598 | 648 | 11.5 |
| $CoCr_2O_4$ | 76.6 | 0.1 | 2.8 | 11.5 | 352 | 469 | 527 | 41.9 |
| $Ce_{0.05}Co_{0.95}Cr_2O_4$ | 116.2 | 0.26 | 3.4 | 8.9 | 329 | 428 | 498 | 54.2 |
| $Ce_{0.1}Co_{0.9}Cr_2O_4$ | 160.5 | 0.42 | 4.9 | 6.4 | 279 | 410 | 485 | 69.8 |
| $Ce_{0.15}Co_{0.85}Cr_2O_4$ | 144.7 | 0.18 | 3.2 | 7.3 | 319 | 443 | 519 | 52.8 |

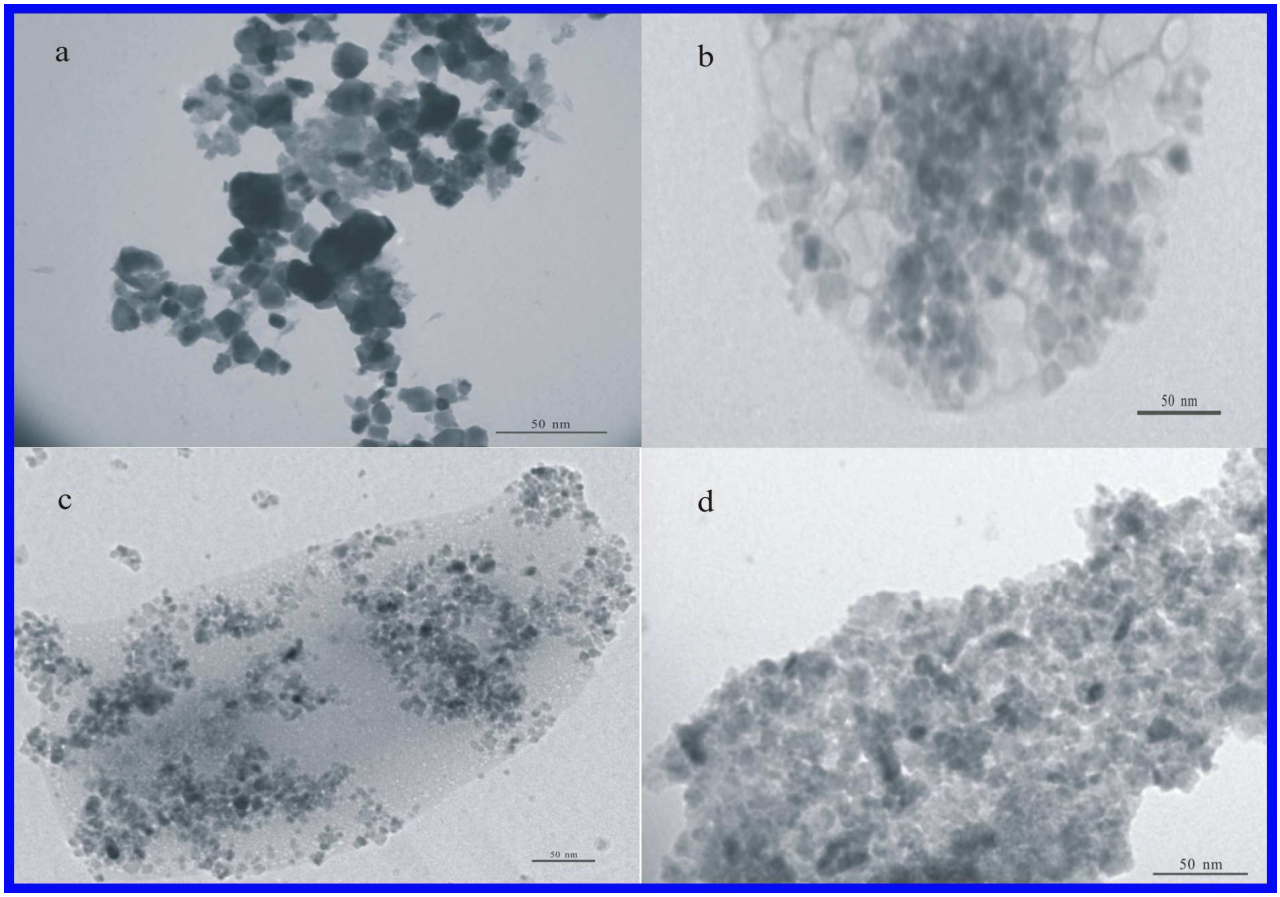


**Fig. 2.** TEM micrograph of the $Ce_xCo_{1-x}Cr_2O_4$ catalyst crystals: a)x=0, (b)x=0.05, (c)x=0.1, (d)x=0.15.

where λ is the X-ray wavelength, taken as 0.154nm, K is the particle shape factor, taken as 0.89, β is defined as the width at half-maximum of the peak, and θ is the position (angle) of the peak. As shown in Table 1, the average crystallite size(D) of catalysts that were determined with the Scherrer equation were much smaller than 15 nm.

Figure 2 shows the TEM images of the $Ce_xCo_{1-x}Cr_2O_4$ catalysts. Figs. 2b~2d show that the crystals of the prepared catalysts are much smaller than 15 nm. In addition, a decrease in the size of the crystallite particles was observed compared to undoped $CoCr_2O_4$ (smaller than 50 nm). As might be expected, the spinel-type oxides produced by the solution combustion synthesis method exhibit more uniform particle sizes. Obviously, these particle sizes are quite uniform and discrete to some extent, which favors an increased number of contact points between the catalysts and the soot, which should accelerate the combustion process of the soot. Interestingly, from the TEM images, the doped samples seem have a large amount of amorphous materials. Since $CoCr_2O_4$ is green colored, the color of our sample is looks black, there must be carbon inside.

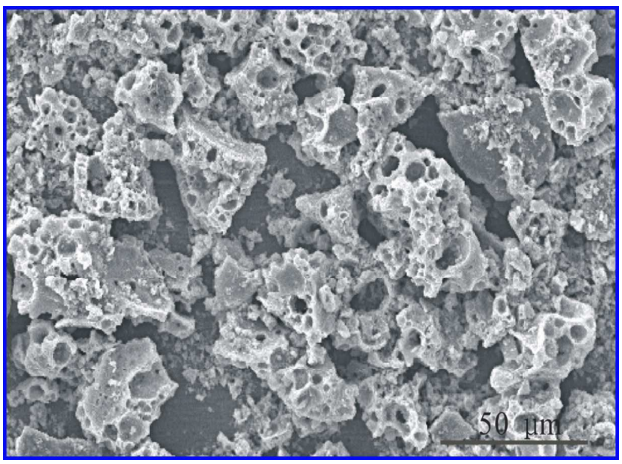


**Fig. 3.** SEM image of the $Ce_{0.1}Co_{0.9}Cr_2O_4$ catalyst crystal agglomerates obtained using the combustion synthesis.

SEM images of the $Ce_{0.1}Co_{0.9}Cr_2O_4$ samples are shown in Fig. 3. The SEM images indicate that the foamy structure of the Ce-substituted samples is quite loose. A foamy microstructure was formed due to the momentary release of gases during the synthesis of the catalyst. Urea, which is more reactive, produces a large amount of gas during combustion, which restricts the particle size and generates more micropores in the final product[15]. Therefore, these results indicate that the foamy structure is a distinctive characteristic of spinel-type catalysts prepared by the solution combustion synthesis method. This foamy structure favors an increased specific surface area for the catalysts,

which means that more surface active sites are available for the simultaneous removal of soot and NOx. However, this microstructure is also advantageous due to its comparatively low pressure drop[20].

In order to further confirm the distribution of Ce in the $Ce_xCo_{1-x}Cr_2O_4$ (x=0, 0.05, 0.1, 0.15) catalysts, micro-zone compositions analysis is performed by Energy Dispersive Spectrometer (EDS). The EDS spectra are shown in Fig. 4 and

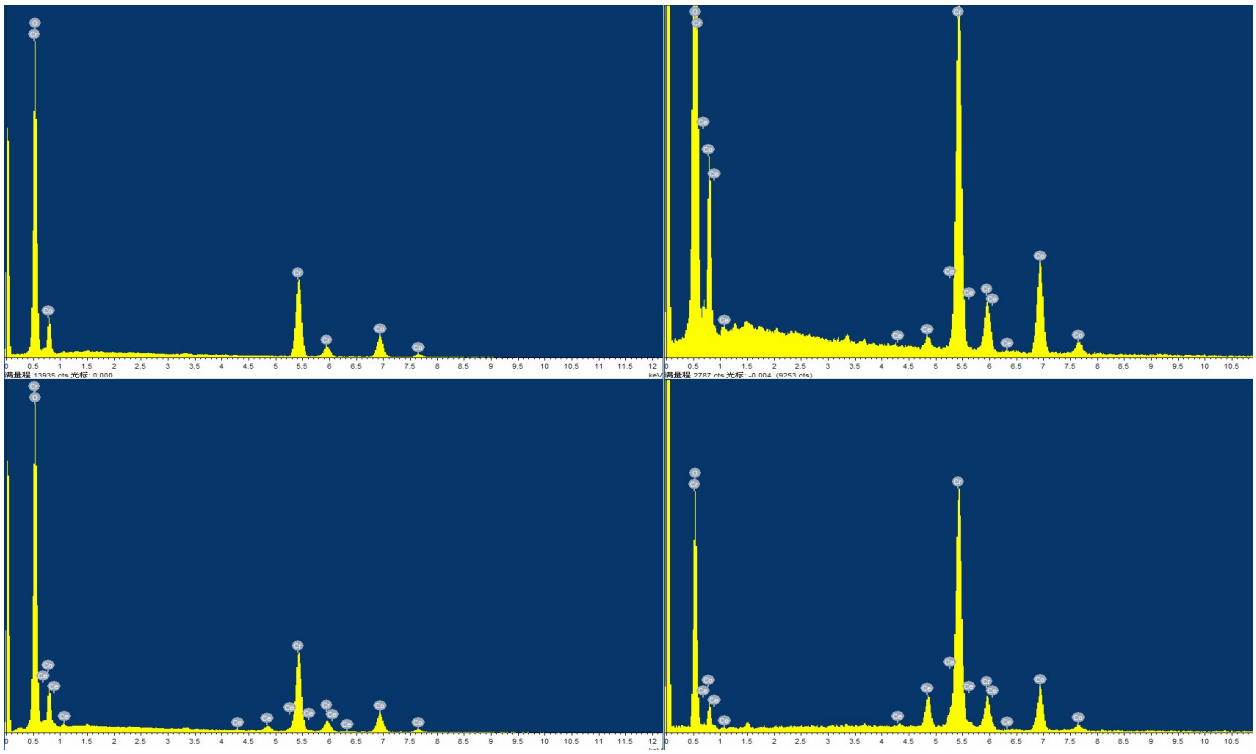

**Fig. 4.** SEM-EDS spectra of the $Ce_xCo_{1-x}Cr_2O_4$ catalysts: a)x=0, (b)x=0.05, (c)x=0.1, (d)x=0.15.

**Table 2.** Metal content of the $Ce_xCo_{1-x}Cr_2O_4$ (x=0, 0.05, 0.1, 0.15).

| element | Atomic concentration(%) | | | |
|---|---|---|---|---|
| | $Ce_xCo_{1-x}Cr_2O_4$ | | | |
| | x=0 | x=0.05 | x=0.1 | x=0.15 |
| Ce | - | 0.5 | 0.94 | 1.46 |
| Co | 9.99 | 9.09 | 8.19 | 7.18 |
| Cr | 19.57 | 18.8 | 18.54 | 19.15 |
| O | 70.43 | 71.61 | 72.23 | 72.21 |

**Table 3.** Repeat the $S_{BET}$ of $Ce_xCo_{1-x}Cr_2O_4$ (x=0, 0.05, 0.1, 0.15).

| $Ce_xCo_{1-x}Cr_2O_4$ | $S_{BET}(m^2/g)$ |
|---|---|
| x=0 | 71.2 |
| x=0.05 | 143.9 |
| x=0.1 | 165.7 |
| x=0.15 | 136.8 |

the corresponding data of EDS spectra are listed in Table 2. The results confirmed that the presence of cerium in $Ce_xCo_{1-x}Cr_2O_4$ (x=0.05, 0.1, 0.15). Therefore, also considering the XRD results (Fig. 4, $Ce^{4+}$ ions enter into the lattice of $CoCr_2O_4$, leading to the diffraction peaks of 2θ position slight increase) and the data of cerium content in Table 2, the cerium is actually completely embedded in the structure of $CoCr_2O_4$. This result implies that the relatively larger $Ce^{4+}$(0.087) ions have been successfully incorporated into the lattice of spinel($CoCr_2O_4$) structure.

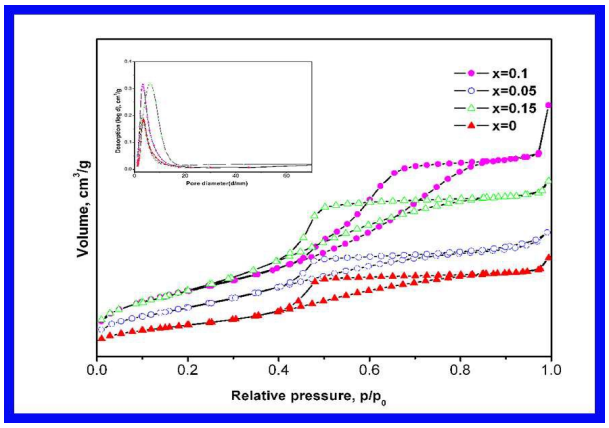


**Fig. 5.** $N_2$ adsorption–desorption isotherms and corresponding pore size Distributions

The $N_2$ adsorption–desorption isotherms for the samples are shown in Fig.5. All of the samples were consistent with typical IV shape isotherms[28] with a well-developed $N_2$ hysteresis loop. Based on the shape of the isotherms of the hysteresis loop, these samples are mesoporous (ranging between 2 and 15 nm). The $N_2$ adsorption–desorption isotherms conforms to class A in accordance with the de Boer classification[29], and the pore structure at both ends of the open cylinder is a distinctive characteristic of these hysteresis loop. From Fig. 4, the $N_2$ adsorption curve of $Ce_{0.1}Co_{0.9}Cr_2O_4$ exhibited the maximum slope for the curve. Therefore, the mesoporous of this sample is the most uniform. Some structural properties of $Ce_xCo_{1-x}Cr_2O_4$ are listed in Table 1. The data indicate that the surface areas of the samples range from 76.6 (x=0) to 160.5 $m^2/g$ (x=0.1). However, when the Ce substitution is greater than 15% (x=0.15), the $S_{BET}$ value begins to decrease slightly. It is well known that a larger surface area can enhance the catalytic activity of the catalysts. The results indicate that the $S_{BET}$ value and pore volumes increased and then decreased as the Ce content increased. This behavior is due to the $Ce_{0.15}Co_{0.85}Cr_2O_4$ particles (smaller than 50 nm) exhibiting easier agglomeration and sintering, which may be caused by agglomeration and sintering of the $CeO_2$ particles at 600℃ for 4 h

when the additional Ce additives result in $CeO_2$ crystals.

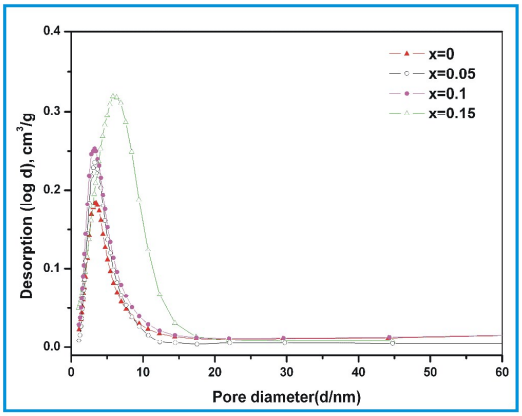


**Fig. 6.** Repeat the pore size Distributions of $Ce_xCo_{1-x}Cr_2O_4$(x=0, 0.05, 0.1, 0.15).

Considering that the mesoporous are come from the space between the aggregation of nanoparticles. In order to investigate the materials is not appropriate mesoporous materials, the repeat test of the $N_2$ adsorption–desorption isotherms for the samples have been performed (are shown in Fig. 6 and Table 3). In fact, the space between the particles does exist. However, if the mesoporous are all come from the space between the particles, then these piled pore are ruleless. The repeat test showed the $S_{BET}$ and the pore-size stable. In this study, these samples are homogenous pore-size distribution (shown in Fig.5. ranging between 2 and 15 nm). Therefore, the mesoporous are major come from the material itself and small come from the space between the particles. It is appropriate to call their materials mesoporous materials.

### 3.2. Catalytic activity assessment

The results for the catalytic removal of PM and NO over $Ce_xCo_{1-x}Cr_2O_4$ (x=0, 0.05, 0.1, 0.15) from 200-600□ in the TPR experiments are shown in Fig. 7 and Table 1. Based on the soot conversion profiles shown in Fig. 7a, all of the catalytic samples are able to decrease the temperature required for soot combustion compared to bare soot (i.e., uncatalyzed reaction). This result indicates that the Ce-doped $CoCr_2O_4$ catalyst exhibits improved catalytic activity. In the temperature range of 200-600□, the concomitant emission of $CO_2$ and reduction of NO indicates that the removal of NO and the soot particulates is occurring simultaneously. In addition, the $Ce_{0.1}Co_{0.9}Cr_2O_4$ catalyst exhibits the highest activity. As shown in Fig. 7, $CoCr_2O_4$ exhibits a high catalytic activity for soot combustion and NO reduction. In comparison to $CoCr_2O_4$, the $T_{50}$ and $T_{90}$ temperature of the soot particulates decreases more

than 80℃ on $Ce_{0.1}Co_{0.9}Cr_2O_4$, and the maximum conversion of NO increases from 41.9% to 69.8%. improves the catalytic activity for the simultaneous removal of soot particulates and NO. In addition,

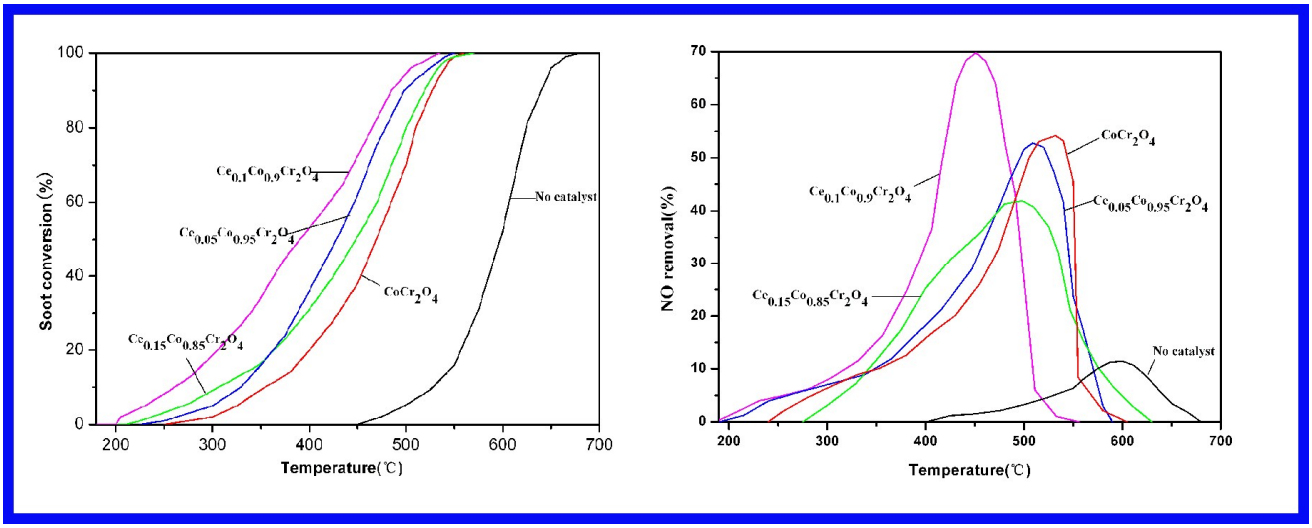


**Fig. 7.** Catalytic conversion as a function of temperature for soot oxidation and NO reduction over the various catalysts.

The high activity for the simultaneous removal of soot particulates and NO by the $Ce_{0.1}Co_{0.9}Cr_2O_4$ catalyst may be due to the increase in the content of over-stoichiometric oxygen and oxygen vacancies resulting from the partial substitution of Ce for Co at A-site ions[30]. The enhancement of the over-stoichiometric oxygen content can improve the mobility of oxygen and promote contact between the soot particulates and oxygen. Zhao et al.[31] reported that the adsorption of NO, which is strongly related to the oxygen vacancy concentration, is significant for the activation of NO. Therefore, the oxygen vacancy concentration when the substitution degree (i.e., x) reaches 0.15, Ce exists in the form of $CeO_2$ instead of entering the $CoCr_2O_4$ lattice, which was confirmed by XRD. Therefore, the surface $CeO_2$ blocks the active sites resulting in two adsorbed $O^-$, which become the primary adsorbed oxygen species on the surface[32]. The results indicated that the $Ce^{4+}$ entering the lattice of $CoCr_2O_4$ improves the catalytic performance. Therefore, the $Ce_{0.1}Co_{0.9}Cr_2O_4$ catalyst exhibits the best catalytic activity.

In order to investigate the stability of the most promising catalyst, five successive catalytic cycles have been performed for soot oxidation and NO

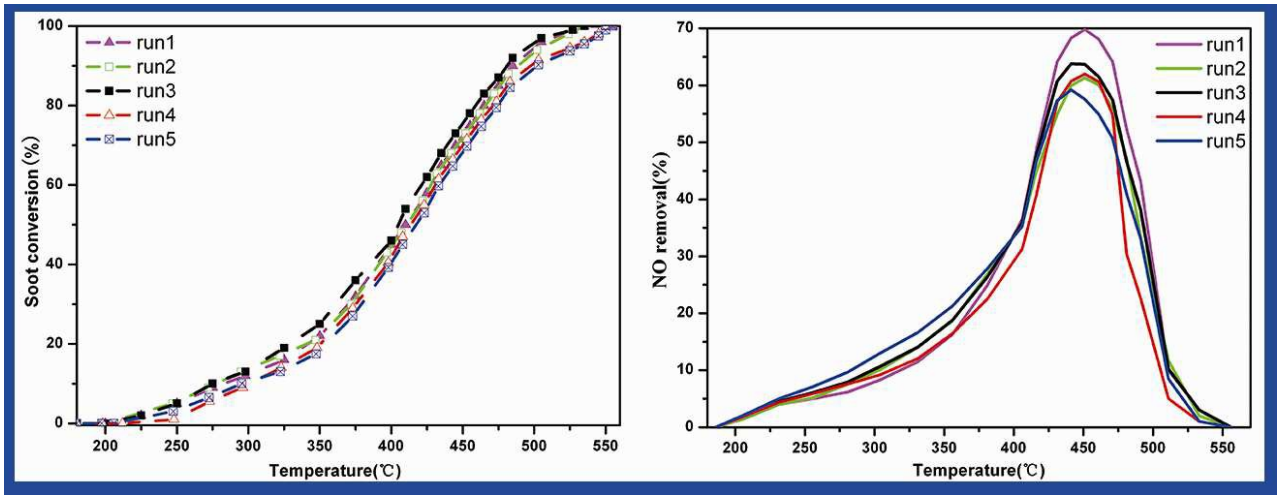


**Fig. 8.** Stability study of the $Ce_{0.1}Co_{0.9}Cr_2O_4$ catalyst for five successive catalytic cycles.

reduction on the $Ce_{0.1}Co_{0.9}Cr_2O_4$. Fig. 8 shows the performances of the $Ce_{0.1}Co_{0.9}Cr_2O_4$ catalyst, as a function of temperature, on each heating run. As a whole, comparable performances have been achieved during five catalytic cycles and no significant deactivation was observed in terms of total soot conversion and NO reduction. Notably, after the third run the catalyst seems to be stabilized in its catalytic activity. Also in that case, a slightly decrease in the catalytic activity was noticed passing from the fourth to the fifth cycle but then the catalytic activity becomes stable and reproducible.

## 4. Conclusions

Using a solution combustion synthesis method, a series of mesostructured catalysts $Ce_xCo_{1-x}Cr_2O_4$ (x=0, 0.05, 0.1, 0.15) were successfully prepared and have a notably foamy structure and fine catalyst crystals (<15 nm). Substitution of cobalt in $CoCr_2O_4$ by cerium in the appropriate amount results in a noticeable influence on the activity of the catalysts for the simultaneous removal of soot and NO. Among all of the catalysts, the best result was obtained with the 10% cerium modified catalyst (i.e., $Ce_{0.1}Co_{0.9}Cr_2O_4$), which exhibited a catalytic activity with a 90% soot conversion and 69.8% NO maximum conversion at 446 °C. This improvement enables the deformation of the spinel structure in the substitution process. Therefore, this deformation results in crystal defects and an increase in the oxygen vacancy concentration, which favors oxygen mobility and the redox



 

behavior of the cerium modified cobalt chromite catalysts.

## Acknowledgments

This work has been supported by the National Natural Science Foundation of China (21277093), Program for New Century Excellent Talents in University (NCET-13-0910), Liaoning BaiQianWan Talents Program (2014921003), the national international scientific and technological cooperative project of China (Grant No. 2011DFR60900) and the Scientific and Technological Planning Project of Jilin Province (Grant No. 20106006), Liaoning province Department of Education fund item (Grant No. L2014477).

## References

[1]R.H. Hammerle, D.A. Ketcher, R.W. Horrock s, G. Lepperhoff, G. Hüthwohl, B. Lüers, SAE Technical Paper No. 942043 (1994).

[2]H. Zhang, F. Gu, Q. Liu, J. Gao, L. Jia, T. Zhu, Y. Chen, Z. Zhong, F. Su, RSC Adv. 2014, **4,** 14879-14889.

[3]S.S. Gill, J.M. Herreros, A. Tsolakis, D.M. Turner, E. Millera, A.P.E. Yorkb, RSC Adv. 2012, **2**, 10400–10408.

[4]X. Chang, G. Lu, Y. Guo, Y. Wang, Y. Guo, Micropor. Mesopor. Mat. 2013, **165**, 113-120.

[5]Y. Peng, J. Li, L. Chen, J. Chen, J. Han, H. Zhang, W. Han. Environ. Sci. Technol. 2012, **46**, 2864-2869.

[6]D. M. Brown, M. R. Wilson, W. MacNee, V. Stone, and K. Donaldson, Toxicol. Appl. Pharm. 2001, **175**, 191-199.

[7]M.V. Twigg, Catal. Today, 2011, **163**, 33-41.

[8]A.G. Konstandopoulos, H.J. Johnson, SAE Paper No. 890405 (1989).

[9]Q. Li, M. Meng, N. Tsubaki, X. G. Li, Z. Q. Li, Y. N. Xie, T. D. Hu, J. Zhang, Appl. Catal. B 2009, **91**, 406-415.

[10]B. Zhao, R. J. Wang, X. X. Yang, Catal. Commun. 2009, **10**, 1029-1033.

[11]P. G. Chen, U. Ibrahim, J. Wang, Fuel, 2014, **130**, 286-295.

[12]K. Ito, K. Kishikawa, A. Watajima, K. Ikeue, M. Machida, Catal. Commun. 2007, **8**, 2176-2180.

[13]D. Fino, N. Russo, G. Saracco, V. Specchia, J Catal. 2006, **242**, 38-47.

[14]M. Zawadzki, W. Walerczyk, F.E. López-Suárez, M.J. Illán-Gómez, A. Bueno-López, Catal. Commun. 2011, **12**, 1238-1241.

[15]P. Stelmachowski, G. Maniak, A. Kotarba, Z. Sojka, Catal. Commun. 2009, **10**, 1062.

[16]S. K. Megarajan, S. Rayalu, Y. Teraoka, N. Labhsetwar, J Mol. Catal. A 2014, **385**, 112–118.

[17]E. Cauda, S. Hernandez, D. Fino, G. Saracco, Environ. Sci. Technol, 2006, **40**, 5532-5537.

[18]J. Chen, W. Shi, Sh. Yang, H. Arandiyan, J. Li, J. Phys. Chem. C 2011, **115**, 17400–17408.

[19]A. Civera, M. Pavese, G. Saracco, V. Specchia, Catal. Today, 2003, **83**, 199.

[20]N. A. Merino, B. P. Barbero, P. Grange, L. E. Cadús, J. Catal. 2005, **231**, 232-244.

[21]Y. Zhang-Steenwinkel, J. Beckers, A. Bliek, Appl. Catal. A 2002, **235**, 79.

[22]J. Li, X. Liang, S. Xu, J. Hao, Appl. Catal. B 2009, **90**, 307.

[23]H. Zhang, J. Han, X. W. Niu, X Han, G. D. Wei, W. Han, J Mol. Catal. A 2011, **350**, 35-39.

[24]S. Letichevsky, C. A. Tellez, R. R. de Avillez, M. I. P. da Silva, M. A. Fraga, L. G. Appel, Appl Catal B, 2005, **58**, 203-210.

[25]R. Si, Y. W. Zhang, S. J. Li, B. X. Lin, C. H. Yan, J Phys. Chem. B 2004, **108**, 12481-12488.

[26]A. Bueno-López, K. Krishna, M. Makkee, J. A. Moulijn, J Catal. 2005, **230**, 237-248.

[27]J. H.Chen, W. B. Shi, J. H. Li, Catal. Today 2011, **175**, 216-222.

[28]K. S. W. Sing, D. H. Everett, W. Haul, L. Moscou, R.A. Pierotti, J. Rouquérol, T. Siemieniewska, J. Macromol. Sci. A 1985, **57**, 603.

[29]T. J. Bandosz, Ch. Lin, J. A. Ritter, J Colloid Interf. Sci. 1998, **198**, 347-353.

[30]J. Y. Luo, M. Meng, X. Li, X. G. Li, Y. Q. Zha, T. D. Hu, Y. N. Xie, J. Zhang, J Catal. 2008, **254**, 310-324.

[31]H. Wang, J. Liu, Z. Zhao, Y. C. Wei, C. M. Xua, Catal. Today, 2012, **184**, 288-300.

[32]L. Xue, C. Zhang, H. He, Y. Teraoka, Appl. Catal. B 2007, **75**, 167.



 